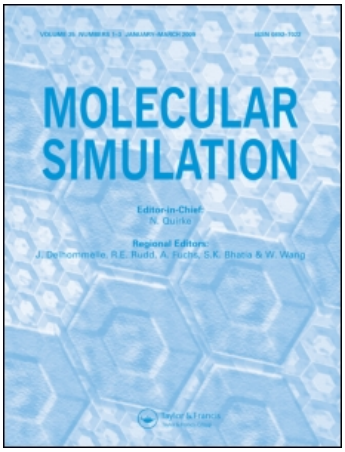

Molecular Simulation

Publication details, including instructions for authors and subscription information:
http://www.informaworld.com/smpp/title~content=t713644482

Molecular Simulations of Phase Transitions in Pores

Keith E. Gubbins[a]; Malgorzata Sliwinska-Bartkowiak[b]; Soong-Hyuck Suh[c]
[a] School of Chemical Engineering, Cornell University, Ithaca, New York, U.S.A. [b] Instytut Fizyki, Uniwersytet im Adama Mickiewicza, ul. Grunwaldzka, Poland [c] Department of Chemical Engineering, Keimyung University, Taegu, South Korea

To cite this Article Gubbins, Keith E. , Sliwinska-Bartkowiak, Malgorzata and Suh, Soong-Hyuck(1996) 'Molecular Simulations of Phase Transitions in Pores', Molecular Simulation, 17: 4, 333 — 367
To link to this Article: DOI: 10.1080/08927029608024116
URL: http://dx.doi.org/10.1080/08927029608024116

Molecular Simulation, 1996, Vol. 17, pp. 333–367
Reprints available directly from the publisher
Photocopying permitted by license only

MOLECULAR SIMULATION OF PHASE TRANSITIONS IN PORES

KEITH E. GUBBINS,[1] MALGORZATA SLIWINSKA-BARTKOWIAK[2] and SOONG-HYUCK SUH[3]

[1]*School of Chemical Engineering, Cornell University, Ithaca, New York 14853, U.S.A.*
[2]*Instytut Fizyki, Uniwersytet im Adama Mickiewicza, ul. Grunwaldzka 6 60–780 Poznan, Poland*
[3]*Department of Chemical Engineering, Keimyung University, Taegu 704–701, South Korea*

(Received December 1995; accepted April 1996)

Methods for simulating phase transitions in narrow pores are reviewed, and the advantages and disadvantages of different techniques are discussed. Examples are given of applications to vapor-liquid, liquid-liquid, melting and freezing, solid-solid and layering transitions. While there has been a considerable body of simulation work on vapor-liquid, wetting and layering transitions for simple fluids and pore geometries, much remains to be done on more complex geometries and network effects, on heterogeneous surfaces, and on liquid-liquid, melting and solid-solid transitions in pores.

Keywords: Phase transitions; pores; capillary condensation; layering transitions; melting; freezing; liquid-liquid equilibria.

1. INTRODUCTION

Fluids confined within narrow pores exhibit a variety of surface-driven phase transitions. Some of these are new (*i.e.* arise solely due to the solid surfaces present), *e.g.* layering, commensurate-incommensurate solid-solid, and wetting transitions; others, *e.g.* melting and capillary condensation, involve surface modification of transitions present in the bulk fluids. The scientific interest in these transitions springs from understanding the novel effects due to the surface forces, and how such transitions (and any associated critical points) are affected by the state conditions and pore variables (pore size and shape, kind of surface, etc.). In addition to the scientific interest, understanding these

phenomena is of great practical importance. Micro- and meso-porous solids are widely used in the chemical, oil and gas, food and pharmaceutical industries for mixture separations, pollution control and as catalyst supports. At present the design of such processes is largely empirical, with little scientific basis. Improved understanding of confinement effects is also needed in connection with many applications in lubrication and adhesion, and in geophysics, geology, and waste cleanup, since many rock and soil formations are porous; the flow, diffusion and selective adsorption of water, aqueous solutions, pollutants, oil and gas in soils and rocks is important in such fields as frost heaving, tertiary oil recovery, gas field technology, and removal of pollutants from ground water and soils.

Some examples of phase transitions in pores are illustrated in Figure 1. The most well-known and widely studied phase transitions are capillary condensation, wetting, and layering transitions. Studies over the last decade using density functional theory [1], molecular simulation [1], and experiments [*e.g.* 2] on well-characterised porous materials have provided considerable insight into the nature of these transitions. Other important transitions that are less studied include melting, solid-solid transitions, solubility phenomena, and liquid-liquid transitions.

Experimental studies of phase transitions in confined fluids is complicated by the difficulty of preparing well characterized porous materials. Simulations therefore offer an important alternative method of study, since the morphology of the porous material is precisely defined. The simulation methods used to study phase transitions in bulk fluids [3–8] are, with little modification, suitable for investigation of phase transitions in pores. However, long-lived metastable states are often a more serious problem in confined systems. These lead to hysteresis effects, the state condition at which the transition occurs being different depending on the direction from which the transition is approached. The determination of the true thermodynamic transition point will often require the calculation of the free energy or chemical potential. A further consideration in studying confined fluids is that it is desirable to know the thermodynamic state of the coexisting bulk fluid or solid. Since the temperature and chemical potential are the same in the bulk and adsorbed phases, this means it is desirable to know or calculate the chemical potential in the adsorbed phase.

In this paper we first briefly consider the most commonly used methods, and then describe several examples taken from recent studies of phase transitions in pores.

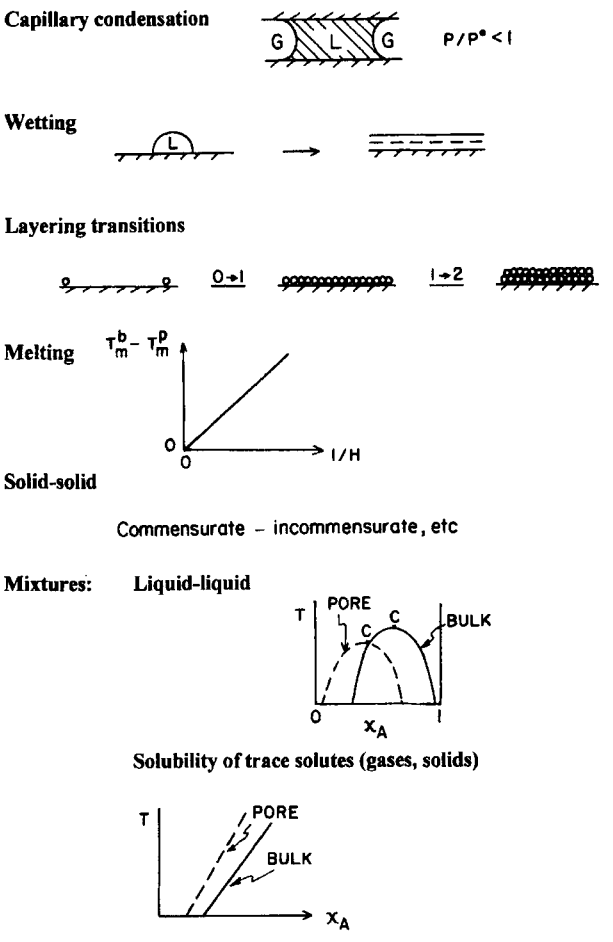

FIGURE 1 Examples of phase transitions in confined systems.

2. METHODS

Phase equilibria in pores, and also the equilibrium between the porous medium and the bulk phase, are governed by equality of temperature and chemical potential:

$$T^\alpha = T^\beta \tag{1}$$

$$\mu_i^\alpha = \mu_i^\beta \quad (i = 1, 2, ...)$$

where i is one of the components of the mixture and α,β are the two phases. Pressure equality is not a requirement since pressure in confined systems is a tensor.

The three most widely used methods for adsorbed systems have been Grand Canonical Monte Carlo (GCMC), Gibbs Ensemble Monte Carlo (GEMC) and Molecular Dynamics (MD) simulations. These each have advantages and disadvantages, as summarized in Table I.

In GCMC simulations the chemical potential values are specified in advance, along with the temperature, so that the values of these are automatically known for both the coexisting phases in the pore and for the bulk phase. It is therefore a natural method to use for confined fluids. If an equation of state is available, it is possible to calculate the pressure of the bulk fluid knowing the chemical potentials. The GCMC method has been widely used to determine adsorption isotherms, heats of adsorption, and phase transitions in pores. Nevertheless, it also has some significant disadvantages. The method (like the GEMC discussed below) runs into difficulties with the molecule insertion step at high densities. An important part of the GCMC procedure involves the attempted insertion of a molecule into one of the phases; if the insertions are made randomly then the number of failed attempts (because the insertion point results in serious overlap with an existing molecule in the pore) rises extremely rapidly as the molecules become densely packed. This difficulty, which is more pronounced for significantly nonspherical molecules, can be overcome by using a biased sampling method [3–8], which attempts to insert the molecules into 'holes' in the fluid, thus improving the chance of successful insertion; the effects of such biasing on the statistical sampling is removed at a later stage. A second disadvantage for many applications is that no information is obtained about the interface itself.

TABLE I Advantages and Disadvantages of Various Methods for Adsorbed Systems

Method	*Advantages*	*Disadvantages*
GCMC	Natural method Know μ, and hence P	Get hysteresis loops Don't see interfaces Fails at high density
GEMC	Get true equilibrium point Fast for mixtures	Don't know μ Don't see interfaces Fails for high density
MD	See interface, phase splitting Get dynamic information	Dont' know μ Difficult for phases of similar density Need large systems

A further difficulty with GCMC (and some other methods) is that hysteresis is found in the calculation of adsorption isotherms where phase transitions occur. If a series of calculations are performed at increasing pressure along an isotherm, for example, the phase transition pressure is often at a different pressure than that observed on reducing the pressure. This results from metastability (local minima in the free energy), and in general neither of the transition points observed in the simulation corresponds to the true thermodynamic transition point [9]. Thermodynamic integration can be used to determine the true transition point. Since the simulation is carried out using the grand canonical ensemble, the appropriate free energy to consider is the grand free energy, $\Omega = -kT \ln \Xi$, where Ξ is the grand partition function. For the bulk fluid $\Omega = -PV$, but for an inhomogeneous fluid (as in a pore) surface terms must be included. For an inhomogeneous fluid containing an interface of area A, classical thermodynamics leads to the identities [10]:

$$\left(\frac{\partial \Omega}{\partial \mu}\right)_{T,V,A} = -N \tag{2}$$

where A is surface area of the system, and

$$\left(\frac{\partial(\Omega/T)}{\partial(1/T)}\right)_{V,A} = U - N\left(\frac{\partial(\mu/T)}{\partial(1/T)}\right)_{V,A} \tag{3}$$

where U is the total internal energy of the system. Restricting eqn. (3) to paths of constant μ yields

$$\left(\frac{\partial(\Omega/T)}{\partial(1/T)}\right)_{V,A,\mu} = U - N\mu \tag{4}$$

For μ low enough that the fluid is an ideal gas,

$$N^{\mathrm{id}}(\mu) = \frac{\exp(\mu/kT)}{\Lambda^3}\int d\mathbf{r} \exp(-V_{\mathrm{ext}}(\mathbf{r})/kT) \tag{5}$$

Substitution of Eqn. (5) into (2) and integrating from zero molecules gives the low density (ideal gas) form for the grand free energy:

$$\Omega^{\mathrm{id}}(\mu) = -kTN^{\mathrm{id}}(\mu) \tag{6}$$

Equations (2) and (4)–(6) can be used to find the grand free energy for any state of interest in the pore. Thus, by carrying out a series of simulations at constant temperature but at varying chemical potential values, Eqn. (2) can be integrated from low density (where $\Omega = \Omega^{id}$ is given by (6)) to the condition of interest. The change in grand free energy on changing to other temperatures can be calculated from Eqn. (4) by carrying out runs at constant chemical potential, but with varying temperature. If, for a given temperature, chemical potential and volume, two states are found, the more stable one is determined as that with the lower Ω. If two such states in the pore have the same Ω they will represent different phases that are in thermodynamic equilibrium. This method has been used [9, 10] to determine capillary condensation coexistence curves.

The GEMC method has the advantage that it determines the true thermodynamic equilibrium point between two coexisting phases in the pore, since the sampling scheme is designed to ensure chemical, as well as mechanical and thermal equilibrium. Thus, hysteresis is not observed. It is also fast, particularly for mixtures, since no interface is involved. However, it suffers from the other two drawbacks of the GCMC method, namely difficulty in molecule insertion at high densities, and failure to observe the nature of the interface. In addition, the chemical potential is not known in advance as in GCMC, and if desired must be calculated by a separate route, *e.g.* the test particle method. Unless this is done, one will not know the state condition of the bulk fluid with which the pore phase is equilibrated.

Molecular dynamics simulations can be used to observe the interfaces between coexisting phases in the pore, and so have this advantage over the GCMC and GEMC methods. One procedure that has proved successful [11] involves first equilibrating the fluid in the pore at a high temperature, above the critical point in the case of gas-liquid or liquid-liquid transitions (or above the range in which the transition of interest occurs in other cases). The simulation is then stopped, the velocities of all the molecules scaled back by a constant factor (chosen to correspond to a suitably lower temperature), and then restarted. The new molecular velocities correspond to a temperature in the two phase region of interest. The fluid in the pore will then separate into the two phases. In general, mechanical equilibrium is quickly reached, whereas chemical equilibrium takes at least one order of magnitude longer, because of the slow diffusion in the dense phases. This quench MD method has the advantage of providing dynamic information about diffusion in the pore and the kinetics associated with the phase separation. Moreover it provides a clear picture of the interface itself, something that cannot be easily studied in the laboratory. The geometry of such interfaces is otherwise unknown, and has

been the subject of debate for several such transitions in pores. Disadvantages of this approach are that it is more work to program than MC, usually requires a larger system and longer runs than GEMC or GCMC, and the chemical potential is not immediately known; the latter can be obtained by the test particle method usually. Also, such phase splitting may be harder to observe very close to critical points, although similar difficulties apply to the GEMC and GCMC techniques.

3. CAPILLARY CONDENSATION AND LAYERING TRANSITIONS

Although many experimental studies of capillary condensation have been reported, relatively few of these have been for well-characterized porous materials with a narrow pore size distribution. An example of a study using such a well-characterized material, sulfur hexafluoride in controlled pore glass, is shown in Figure 2 [2]. These materials have a very narrow pore size distribution in the mesoporous range, so that the phase transition is quite sharp. The effect of confinement is to shift the coexistence curve to lower

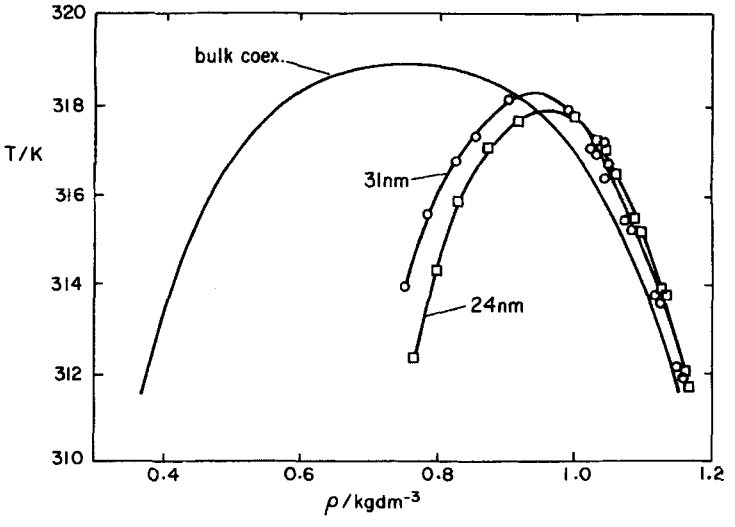

FIGURE 2 Vapour-liquid coexistence curves for sulphur hexafluoride as bulk fluid and as adsorbed fluid in controlled pore glass of two different mean pore diameters. The abscissa shows the density averaged across the pore diameter in the case of the pore fluids. The coexistence curves are shited to lower temperature and higher density in the pore fluids. From Thommes and Findenegg [2].

temperatures and to higher mean densities. The much higher density for the low density phase in the pore is a result of layer formation on the walls. The downward shift in the pore critical temperature was found to be 0.92 ± 0.24 K for the glass with 24 nm mean pore diameter, and 0.48 ± 0.23 K for the 31 nm mean pore width.

Since about 1986 there have been numerous simulation studies of capillary condensation in pores of simple geometry, *e.g.* slits and cylinders, and several studies of layering transitions. These are too numerous to review here, but a cross-section of examples of studies of this type can be found in the proceedings of the International Conferences on the Fundamentals of Adsorption, held every three years [1]. Most of these simulations have employed the GCMC method, but several use either GEMC or MD. In this section we show several examples drawn from this literature.

In Figure 3 we show results of GCMC simulations [10] for the adsorption of a Lennard-Jones fluid (the potential cut and shifted at $r_c = 2.5\sigma$) modeled on methane in slit graphite pores of width $H^* = H/\sigma = 5$. The pore width is defined as the distance between the nuclei of carbon atoms in the first layer of each of the two opposing walls, and the solid-fluid interaction was modeled using the (10, 4, 3) potential [12]. From Figure 3(a) we see a first order layering transition ($0 \rightarrow 1$ layers) at $\mu^*_{con} = -10.0$ for $T^* = 0.4$. This becomes a continuous transition for the higher temperatures, the increase in adsorption becoming less steep with increasing temperature. This transition corresponds to the formation of a single adsorbed fluid-like layer on each wall. The behavior of the isotherm at $T^* = 0.5$ suggests that the critical temperature for this transition is slightly below 0.5. This is in good agreement with the experimental results of Kim *et al.* [13], which show the submonolayer critical temperature of methane on graphite to be 68.8 K ($T^* = 0.46$). There is no observable hysteresis associated with this layering transition. At higher chemical potentials around $\mu^*_{con} = -6.0$, for temperatures in the range $T^* = 0.4 - 0.7$ the adsorption isotherms undergo first order jumps, but are continuous for the higher temperatures of $T^* = 0.8$ and above. These jumps correspond to the formation of a second, inner layer on each wall. Since a pore of $H^* = 5$ can only hold four layers, these transitions represent capillary condensation. Hysteresis is associated with this transition, the hysteresis loop becoming smaller with increasing temperature and disappearing at $T^* = 0.7$. For the temperatures of $T^* = 0.4, 0.5, 0.6$ and 0.7 the true thermodynamic phase transition (two phases having equal grand potentials) was determined by integration of eqn. (2) using the boundary condition of eqn. (6). For still higher chemical potentials, around $\mu^*_{con} = -4.0$, all of the adsorption isotherms approach a limiting adsorption corresponding to completely filled pores. Freezing transitions (marked FT) are

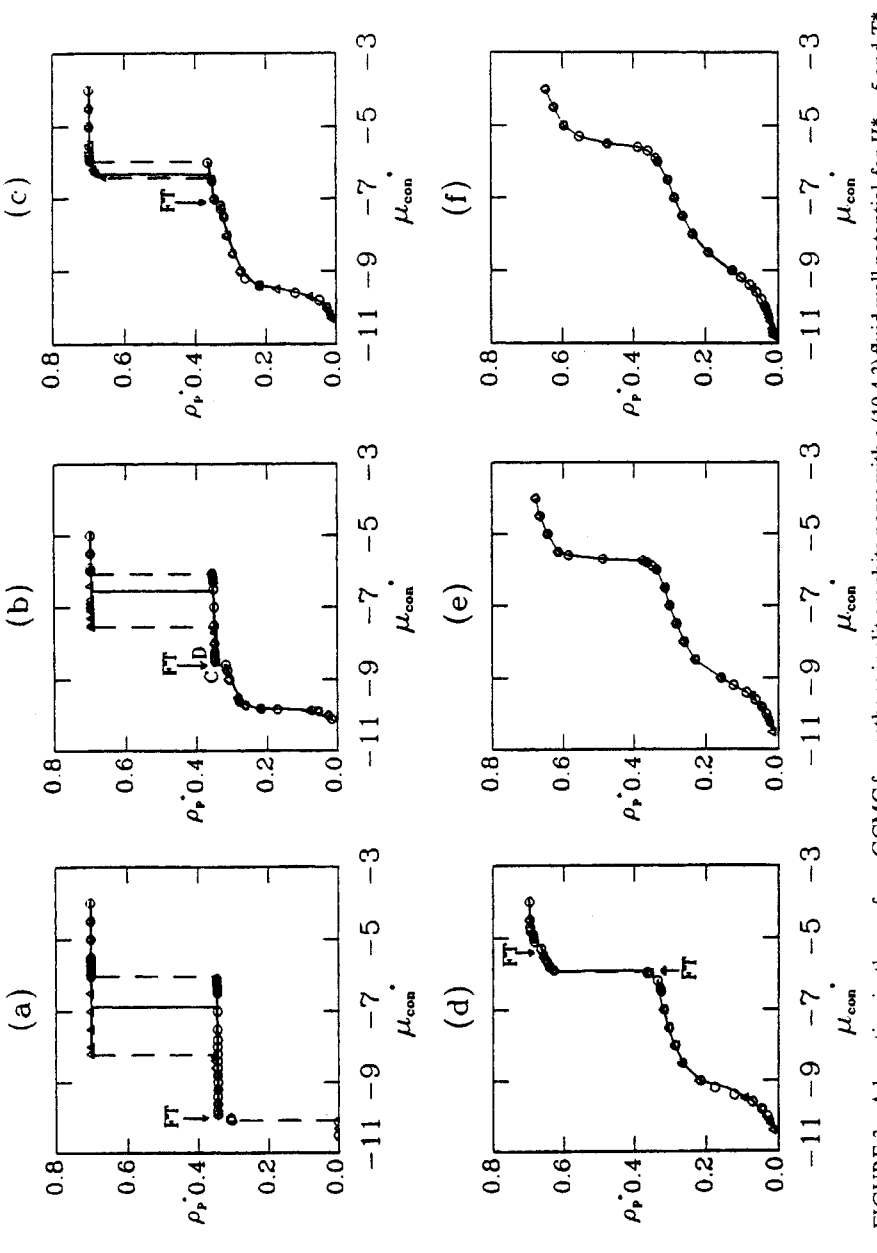

FIGURE 3 Adsorption isotherms from GCMC for methane in slit graphite pores with a (10,4,3) fluid wall potential, for $H^* = 5$ and T^* values of: (a) 0.4, (b) 0.5, (c) 0.6, (d) 0.7, (e) 0.8, and (f) 0.9. The adsorption plotted is the average fluid number density in the pore, $\rho^*_p = \rho_p\sigma^3$, reduced with the methane potential parameter σ. Adsorption is denoted by circles, desorption by triangles, first-order transitions as dashed lines, and the true thermodynamic phase transition as a solid line. FT stands for freezing transition. From Jiang *et al.* [10].

also observed at the lower temperatures shown in Figure 3. These are further discussed in the section on freezing and melting below.

For larger pores, further layering transitions are found. Adsorption isotherms for $H^* = 10$ and 20 at $T^* = 0.5$ are shown in Figure 4. For $H^* = 10$ the formation of three layers are observed on adsorption, followed by capillary condensation. For $H^* = 20$ four layers are formed prior to capillary condensation. As for the smaller pores the $0 \rightarrow 1$ transition is continuous, whereas the $1 \rightarrow 2, 2 \rightarrow 3$ (and $3 \rightarrow 4$ for $H^* = 20$) transitions appear to be first order. A large hysteresis loop encompassing the $1 \rightarrow 2$ and higher transitions is observed; since the grand potentials were not computed for these transitions the true thermodynamic transitions are unknown, and it is possible that some of these apparent transitions are metastable.

An example of the use of quench MD to study vapor-liquid transitions in cylindrical pores is shown in Figure 5. The intermolecular potentials are Lennard-Jones models, cut and shifted at $r_c = 2.5\sigma$, with parameters chosen to model argon fluid in a carbon dioxide pore [9, 11]. Strictly, it is not correct to talk of phase transitions in a cylindrical pore, since finite size rounding effects will blur the transition. However, such effects are known to be very small for

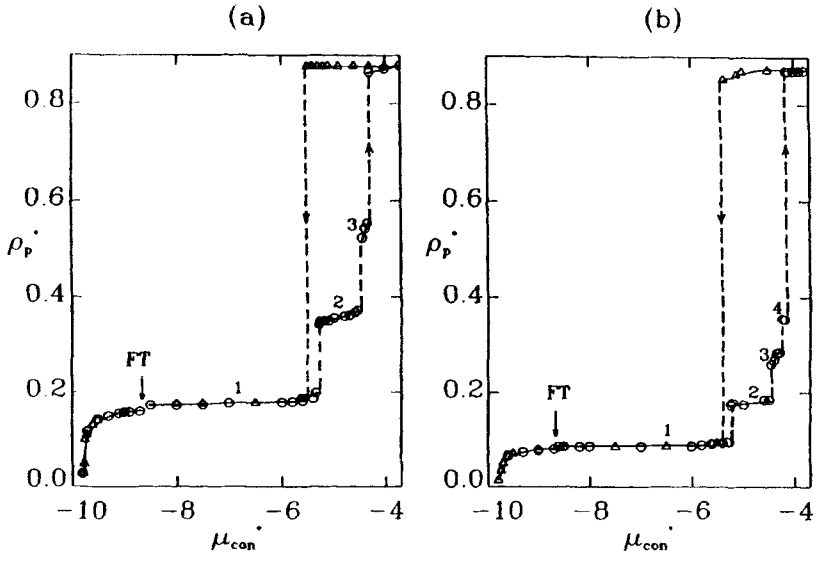

FIGURE 4 Adsorption isotherms from GCMC simulations for the same system as in Figure 3, but for $T^* = 0.5$ and (a) $H^* = 10$, (b) $H^* = 20$. Adsorption is denoted by circles, desorption by triangles, and first order transitions as dashed lines. FT is freezing transition. From Jiang *et al.* [10].

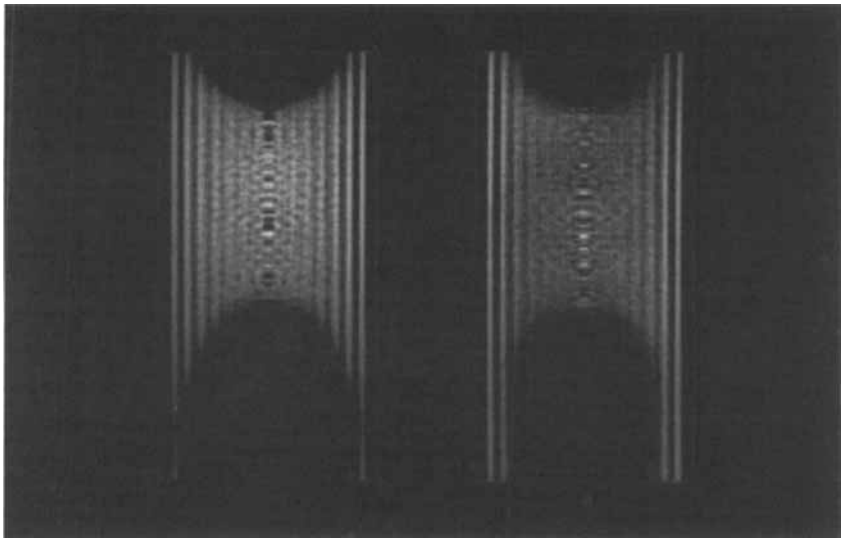

FIGURE 5 Density profiles for a Lennard-Jones fluid (modeled on argon) in a cylindrical pore (modeled on CO_2) of radius $R^* = R/\sigma = 7.5$ at T/T_c values of 0.631 (left) and 0.766 (right), obtained by quench MD. Intensity is proportional to the density; dark areas correspond to gas phase. From Heffelfinger *et al.* [11].

the pore sizes considered here. In Figure 5 the average fluid densities in various parts of the pore are shown. Brightness is proportional to fluid density in these pictures, so that the dark regions are the gas phase. The bright bands shown correspond to peaks in the density profile. After quenching phase separation is extremely rapid, leading to a liquid phase that is separated from the gas one by a (roughly) hemispherical meniscus. This process is analogous to spinodal decomposition in bulk fluids, as observed by Abraham *et al.* [14]. In Figure 5 the meniscus is seen to broaden with increasing temperature, and for the higher temperature the adsorbed layer near the wall grows. Just above the pore critical temperature large density fluctuations are usually observed [11].

The coexistence curve for this system for a radius of $R^* = 5.0$ is shown in Figure 6. In plotting Figures 5 and 6 the pore diameter is defined as the distance between opposing walls, taken to be at the point where the fluid-wall potential diverges to infinity. This definition includes some dead space near the walls, so that the pore volume so defined will be greater than the volume accessible to the centers of fluid molecules. As a result, for small pores the coexistence curves will be shifted towards lower densities than would otherwise be the case. The results shown are obtained by quench MD, but are in excellent agreement with independent calculations using GCMC. The main

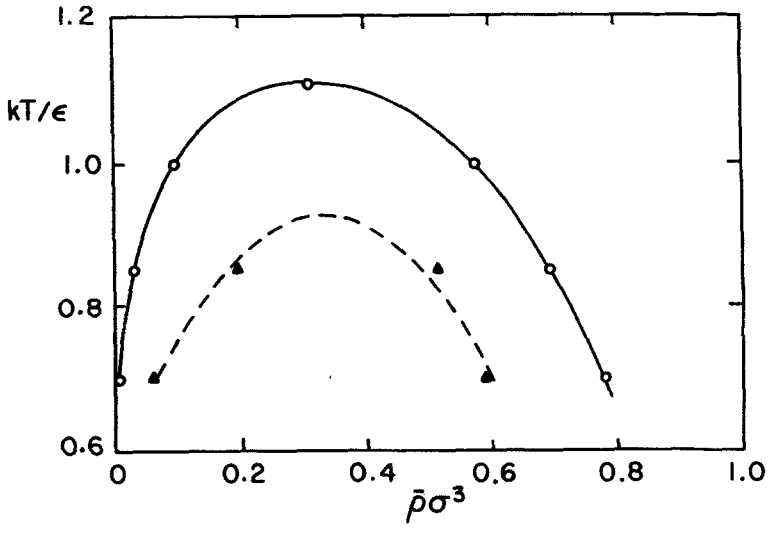

FIGURE 6 Phase diagram for argon in the cylindrical pore system of figure 5, for a radius $R^* = R/\sigma = 5.0$ (dashed line and triangular points). The abscissa represents the average (reduced) number density in the pore. The bulk coexistence curve (solid line), plotted against the bulk density, is shown for comparison. From Heffelfinger *et al.* [11].

effects of confinement are a lowering of the critical temperature, and an increase in the density of the gas phase due to strong adsorption on the pore walls.

Most simulations have been for pores that are (via the boundary conditions) infinitely long. If the pore is open at each end and of moderate length, end effects can be significant. An example is shown in Figure 7, where adsorption isotherms obtained by GCMC simulation [15] are compared for two model double-buckytubes (cylindrical pores of graphitic carbon, with walls consisting of two graphitic layers) of internal diameter 4.78 nm; one of these tubes is infinite in length and the other is an open-ended tube of length 7.7 nm. While molecules in the central region of the open-ended buckytube are unaware of the tube ends, those within about 2 nm of the ends experience a reduction in the fluid-wall interaction. For an adsorption below about 7 mmol g^{-1}, the open-ended and infinite tubes adsorb in an almost identical manner. However, the phase transition region for the two cases are markedly different. For the open-ended tube the transition occurs at a higher pressure, as expected, a result of the reduced fluid-wall interaction in the end regions. The infinite tube shows a hysteresis loop that covers a much broader pressure range, with discontinuous capillary evaporation at a reduced pressure of about 0.2. By

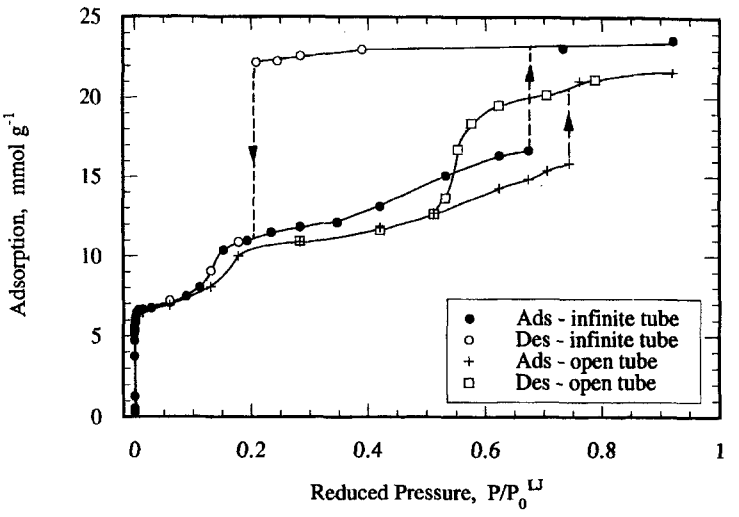

FIGURE 7 Adsorption isotherms for (Lennard-Jones) argon in double-buckytubes of internal diameter 4.78 nm at 77 K. Results are shown for a tube that is infinitely long, and for an open-ended tube of length 7.7 nm. From Maddox and Gubbins [15].

contrast, the open-ended tube shows a much narrower hysteresis loop, which is also more rounded, and without first order capillary evaporation on desorption. This latter isotherm is more reminiscent of most experimentally observed isotherms. Snapshots of typical equilibrium configurations show a gas-liquid meniscus at the ends of the open-ended tube when it is full of adsorbed fluid [15]. It is clear that the capillary critical temperature will be significantly affected by pore length.

The examples cited above involve homogeneous surfaces. Pore filling proceeds by the formation of adsorbed layers on the wall; layering transitions occur in some cases (low temperature, strong fluid-wall interaction), followed at some higher pressure by capillary condensation. For heterogeneous surfaces having active energetic sites, the pore filling mechanism is often qualitatively different. Such energetic sites can be due to chemical groups fixed to the surface, for example oxygenated groups (hydroxyl, carboxyl, carbonyl, etc.) that can form H-bonds with suitable adsorbate molecules (*e.g.* water, alcohols, amines); or they can be due to defects in the surface, pores of varying geometry, constrictions in the pores, etc. In such cases the adsorbate molecules tend to cluster in the energetically favorable sites, rather than adsorb in uniform layers. Capillary condensation may or may not occur, depending on the density of active sites and the strength of the adsorbent/adsorbate interaction.

An example of such behavior is illustrated in Figures 8–11, for a system modeled on water in an activated carbon pore [16]. The water molecules are modeled as Lennard-Jones spheres with four, tetrahedrally arranged H-bonding sites, modeled as off-center square well interactions; the well depth of these sites was $\varepsilon_{HB}/kT = 12$. Two of these sites correspond to the H atoms, and the other two to the lone pair electrons. The pore is modeled as a graphite surface, modeled with the (10,4,3) potential [12], on which are placed square well sites with parameters chosen to mimic sites such as COOH (Fig. 8); these sites are placed at a distance $z = 0.5\sigma_{ss} = 0.17$ nm above the surface (defined as the plane through the centers of the C atoms in the first layer of the solid), where σ_{ss} is the Lennard-Jones parameter for the solid C interaction. The square well parameters for the wall sites were taken to be equal to those for the water molecules. The adsorption behavior was studied by GCMC simulations as a function of the pressure, surface density of active sites, and geometric arrangement of sites [16]. Long runs are needed (typically 50×10^6 configurations were used) in order to ensure ergodicity, since otherwise the strong adsorbate/active site interactions could lead to H-bonds that are unlikely to be broken during the course of the simulation. For values of $\varepsilon_{HB}/kT = 12$, GCMC simulations are feasible, but for much stronger bonding strengths it is necessary to use biased sampling methods [17–20]. In Figure 9 the adsorption behavior of simple models of water (closed circles) and propane (squares) in a graphitic (no active sites) carbon pore of width $H = 6$ nm are compared at 300 K. The model described above was used for water, and a spherical

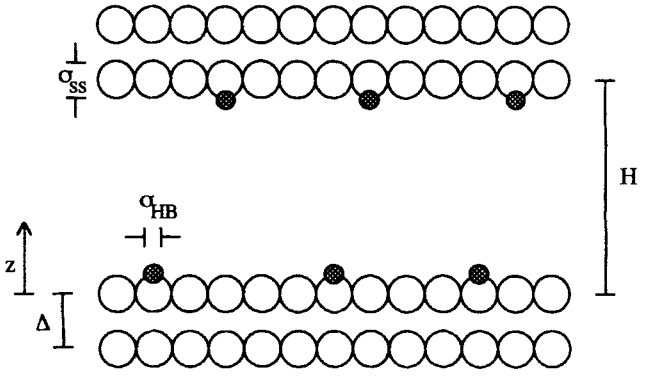

FIGURE 8 Lateral view of pore geometry for model activated carbon. Periodic boundary conditions are used in the x (from left to right) and y (in and out of the page) directions. Open circles represent the C atoms forming the walls of the pore, shaded circles represent the activated (square-well) sites. From Muller and Gubbins [16].

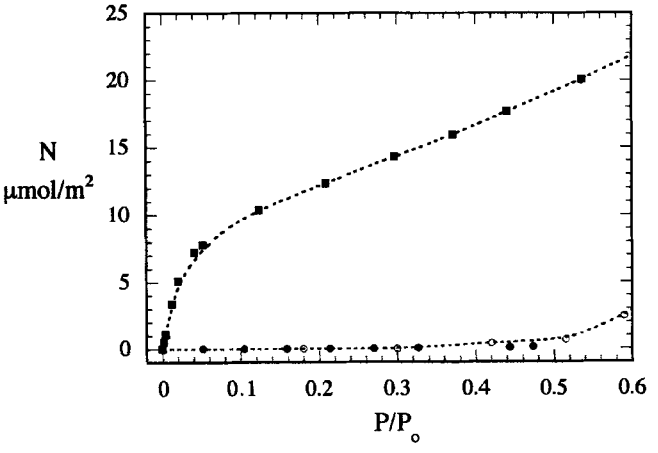

FIGURE 9 Adsorption isotherms for models of water (solid circles) and propane (solid squares) in a graphitic carbon pore of width $H = 6$ nm at 300 K, from GCMC simulations. Open circles are experimental results for water on Graphon at 20° C from Walker and Janov [21]. From Müller and Gubbins [16].

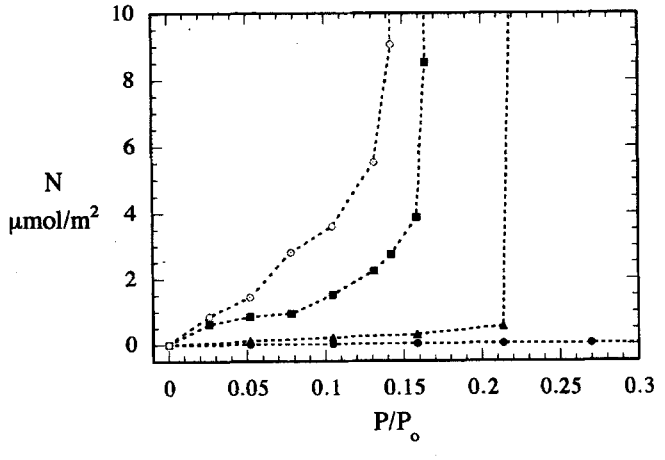

FIGURE 10 Adsorption isotherms for water in an activated carbon pore of $H = 6$ nm at 300 K from GCMC simulations. Curves shown are for $n = 0$ (closed circles), 0.222 (triangles), 0.444 (squares) and 1.000 (open circles) sites/nm^2. From Müller and Gubbins [16].

Lennard-Jones model was used for propane. While propane adsorbs strongly at low pressure, almost no water is adsorbed except at relatively high pressures, in agreement with the experimental results [21]. The influence of varying the density of active sites is shown in Figures 10 and 11. The isotherms

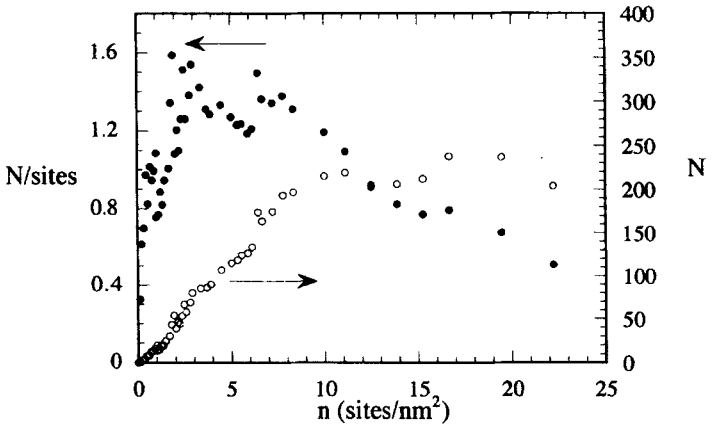

FIGURE 11 Adsorption as a function of site density, n in sites/nm^2, for a pore of $H = 2$ nm at 300 K and a reduced pressure of $P/P^\circ = 0.0419$. Open circles (right ordinate) are the number of water molecules adsorbed, N. Closed circles (left ordinate) are the number of molecules adsorbed pet active site. From Müller and Gubbins [16].

shown in Figure 10 are for active sites placed randomly on the carbon surfaces, with densities of $n = 0$, 0.222, 0.444 and 1.0 sites/nm^2. For $n = 0$ and for $n = 0.222$, there is little adsorption for lower pressures, followed by capillary condensation. The condensation pressure is shifted to considerably lower pressures by the presence of the active sites. For the higher site densities, $n = 0.444$ and 1.0, the pore filling pressure is further shifted to lower pressures, and the filling mechanism changes. Capillary condensation is no longer observed at these site densities. As pressure is increased, water molecules adsorb on the active sites and then form clusters around these sites. Adsorption is much enhanced if the sites are placed so that the water molecule clusters can form bridges between two or more sites [16]. Eventually the pore fills, but without any sharp transition. Varying the geometry of the placement of the sites, keeping the average site density constant, is found to have a marked effect on the adsorption [16], since there are strong collective effects due to the bridging phenomenon. The effect of varying the site density at fixed relative pressure ($P/P^\circ = 0.0419$) and temperature (300 K) is shown in Figure 11. At low site densities ($0 < n < 3$) the number of water molecules adsorbed is proportional to the number of sites. At such low site densities the sites are sparsely located and there is less chance of cooperative effects. For sufficiently high site densities ($n > 7$) the addition of further sites has little effect on the adsorption of water. For such site densities both pore walls are covered by water molecules, effectively screening any attraction from the walls or the

remaining unoccupied sites. Site densities for many activated carbons seem to range from 0.2 to about 2 sites/nm^2 [*e.g.* 22,23]. For comparison, the density of carbon atoms on the surface is about 38.2 atoms/nm^2.

4. LIQUID-LIQUID EQUILIBRIA

Liquid-liquid transitions in pores are important in connection with oil recovery, lubrication, coating technology and pollution control. The influence of confinement on solubilities is of interest in understanding the dispersion of pollutants in soils, in removing trace pollutants from water, and in lubrication.

There have been very few experimental studies of liquid-liquid transitions for well-characterized porous materials so far. Recently, Sliwinska-Bartkowiak and coworkers have measured liquid-liquid equilibrium (LLE) coexistence curves in controlled pore glasses using nonlinear dielectric, as well as optical methods [24, 25]. Their results for nitrobenzene(1)/*n*-hexane(2) mixtures in a glass with pores of diameter 100 nm show a shift in the *T*-*x* coexistence curve towards the hexane-rich side, with decreased solubility of the nitrobenzene in the hexane-rich phase, and increased solubility for the hexane in the nitrobenzene-rich phase (Fig. 12). Thus, even for such large pores, there is a noticeable shift in the coexistence curve, the critical composition shifting from $x_1 \approx 0.42$ in the bulk mixture to 0.38 in the controlled pore glass. Any effect on the critical temperature is not observable at these large

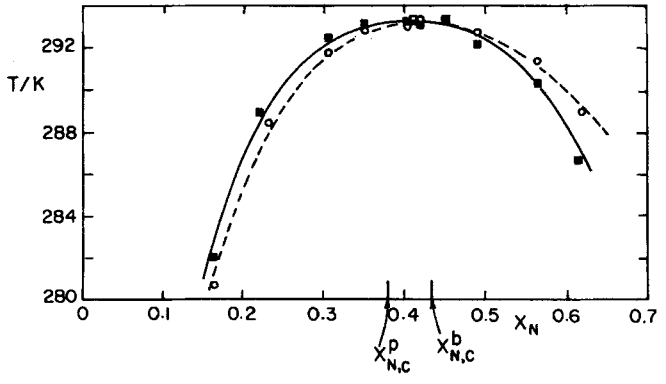

FIGURE 12 Liquid-liquid coexistence curves for mixtures of nitrobenzene (N) and *n*-hexane. Dashed line and o points are data for the bulk mixture; solid line and ■ points are for the mixture confined in a controlled pore glass with average pore size of 100 nm. From Sliwinska- Bartkowiak *et al.* [25].

pore diameters. Solvation force measurements by Christenson and Blom [26] suggest they may have observed liquid-liquid phase separation in a mixture of water and octomethylcyclotetrasiloxane (OMCTS). They apparently observed liquid-liquid immiscibility for a composition corresponding to a homogeneous phase in the coexisting bulk liquid mixture; this implies that the solubilitiy of OMCTS is less in the pore than in the bulk. However, their results did not produce the coexistence curve for liquid-liquid equilibrium (LLE) in the pores. LLE has also been studied in thin films of polymer blends [27–29], and it has been found that, in addition to a shift in the coexistence curve to different compositions, the LL critical temperature is shifted, the nature of the shift depending on the component of the blend that adsorbs most strongly on the surfaces. For such polymer blends, shifts in the coexistence curve are found even for pores as large as 1 μm (1000 nm). So far these experimental studies of LLE for both simple and polymeric fluids are not sufficiently advanced to provide any systematic picture of the effects of confinement. At present no simple physical picture exists to explain the effects of confinement on LLE or solubility, in contrast to the situation for capillary condensation and melting. In addition to this work on well-characterized pores, there is a body of experimental work on LL phase separation near the critical mixing point for more random pore structures [see ref. 30 and references therein]; much of the interest in these studies is the possibility of random field behavior due to the interconnected pore network.

Molecular simulation studies of liquid-liquid equilibria in pores of slit shape have been carried out for symmetrical mixtures recently [31, 32]. The fluid is a Lennard-Jones (LJ) binary mixture, in which the like pair interactions, u_{11} and u_{22} are identical ($\varepsilon_{11} = \varepsilon_{22}$, $\sigma_{11} = \sigma_{22}$), while the attractive part of the unlike pair interaction u_{12} is considerably weaker than the geometric mean of the like pair interactions ($\varepsilon_{12} = \xi_{12}(\varepsilon_{11}\varepsilon_{12})^{1/2}$, $\sigma_{12} = \sigma_{11} = \sigma_{22}$, where ξ_{12} is much less than unity). The weak unlike pair interaction leads to liquid-liquid immiscibility in the bulk mixture, and the symmetry of the potential produces a liquid-liquid coexistence curve that is symmetrical about $x_1 = 0.5$, a homogeneous positive azeotrope at $x_1 = 0.5$ at higher pressures, and a heterogeneous azeotrope at low pressures. We refer to this model mixture as the *symmetrical LJ mixture*. The phase behavior of this symmetric mixture is established via molecular simulation and DFT studies for the bulk fluid [33–36]. Components 1 and 2 were also symmetrical with respect to their interaction with the pore walls in these studies, so that the pore fluid coexistence curves should also be symmetrical with respect to $x_1 = 0.5$. The models used in the two studies [31, 32] differed in detail. The unlike pair parameter ξ_{12} was 0.75 in the study of Kierlik and coworkers [32], and 0.65 in

that of Gózdz *et al.* [31], leading to a more nonideal solution in the latter case and a higher critical solution temperature. Kierlik and coworkers chose a (9,3) fluid-wall interaction model with the parameters chosen to model argon as the fluid and a carbon dioxide wall; Gózdz *et al.*, used a (10,4,3) interaction model for methane on carbon [12]. Kierlik *et al.*, used Grand Canonical Monte Carlo (GCMC) simulations and density functional theory, while Gódz *et al.*, used the Gibbs Ensemble Monte Carlo (GEMC) method. Since the 1 and 2 molecules are identical in these symmetrical mixtures, it is possible to use molecule exchange in place of the molecule insertion step, thus greatly simplifying the simulations at these high densities [31]. The results from the two groups are similar, and typical coexistence curves are shown in Figures 13 and 14. The main conclusions from these studies are that confinement of these symmetric mixtures leads to: (a) a decreased region of immiscibility (*i.e.* selective adsorption of the dilute component), and (b) a lowering of the critical solution temperature. The decreased immiscibility range in the pore suggests that the effect of the weak unlike pair interaction is reduced as a result of the reduced dimesionality associated with decreased pore size. These effects seem to be in agreement with the limited amount of experimental data that exists so far [24–29].

A similar study using GEMC simulations for a symmetric mixture of chain molecules (of length 20 LJ monomer units) has been reported by Kumar *et al.* [37]. As for the LJ symmetric mixture described above, like pair interactions were the same for the two species, but the monomer LJ interactions for the unlike molecule pair interactions were weaker ($\xi_{12} = 0.9$). Confinement was found to lead to a reduction in the range of immiscibility, and to a decrease in the critical mixing temperature, as for the simple LJ fluid. The LL coexistence curves found for this symmetric chain molecule mixture were qualitatively similar to those shown in Figures 13 and 14.

All of the results discussed above are for a mixture that is symmetric with respect to both the fluid-fluid and fluid-solid interactions. Recently, density functional theory calculations have been reported [25] for a LJ mixture in which the fluid-fluid interactions are symmetrical as above, but the fluid-wall interactions are different for species 1 and 2. The Rosenfeld-Kierlik-Rosinberg theory was used, and the influence of varying the fluid-wall well depth for the two species was examined, with species 2 being more strongly attracted to the wall than species 1. It was found that this resulted in a shift of the coexistence curve towards the 2-rich side. The predicted shift is qualitatively similar to that observed experimentally for the nitrobenzene/n-hexane mixtures [24,25]. More work is needed to fully understand these effects, particularly for unsymmetrical mixtures and pores.

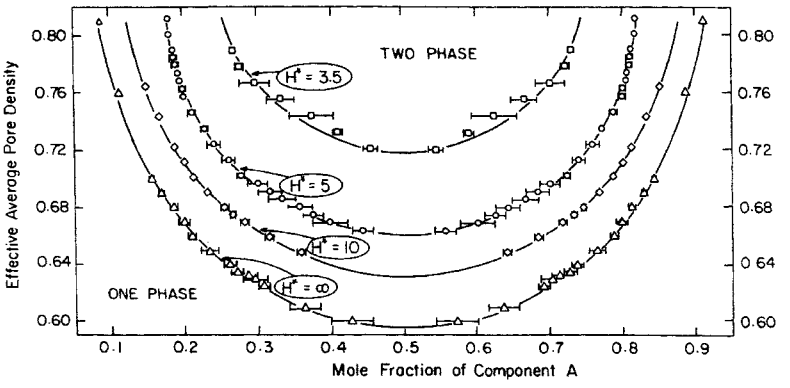

FIGURE 13 Liquid-liquid equilibrium coexistence curves for a symmetrical LJ mixture in slit pores of width H ($H^* = H/\sigma$) at a fixed temperature $T^* = 1.2$ and various bulk pressures, by GEMC. From Gózdz *et al.* [31].

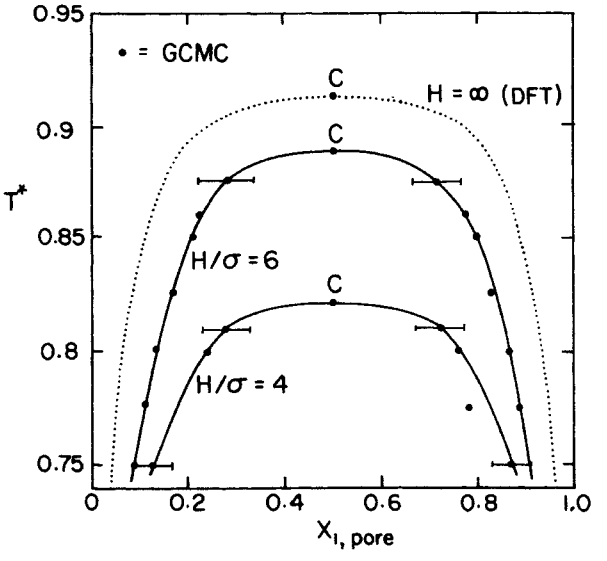

FIGURE 14 Liquid-liquid equilibrium coexistence curves for a symmetrical LJ mixture in slit pores of width H ($H^* = H/\sigma$) at fixed pressure, from Kierlik *et al.* [32].

5. MELTING/FREEZING TRANSITIONS

Freezing and melting transitions in pores are of importance in frost heaving, in the distribution of pollutants in soils, in the formation and decomposition of gas hydrates, in the manufacture of nanomaterials, and in other manufacturing processes. Several experimental studies of melting and freezing in well-characterized porous materials have been reported [38–46]. In general these show that the melting point is lowered on confinement, and that hysteresis is associated with the transition. Typical results are shown in Figure 15 (a), which gives the lowering of the freezing temperature for oxygen in well-characterized sol-gel glasses having a narrow pore size distribution, as determined by a picosecond optical technique [39]. The pore radii ranged from 2.2 to 18.7 nm. A significant lowering of the freezing temperature is found, the depression being as large as 10 K for the smallest (2.2 nm) pores. Melting temperatures were higher than those for freezing, indicating strong hysteresis effects. Particularly large effects on the freezing and melting temperatures for indium in porous silica glasses have been reported [43], the melting point depression for the smallest pores of about 6 nm diameter being about 47 K, as shown in Figure 15 (b). For the melting of indium in 8.2 nm controlled pore glass, the latent heat was determined to be 10.2 ± 0.4 J/g, much lower than the bulk fluid value of 28.4 J/g. Similar results have been found for other fluids. For example, Molz *et al.* [44] obtained the following results for freezing and melting temperatures for oxygen and argon in a porous silica xerogel with mean pore diameters of about oxygen and argon in a porous silica xerogel with mean pore diameters of about 3.6 nm, using heat capacity measurements:

Transition	*Pore Freezing*	*Pore Melting*	*Bulk*
Oxygen, solid-liquid	47.5 K	49.1 K	54.4 K
Oxygen, solid-solid	36.0	40..5	43.8
Argon, solid-liquid	72.3	74.8	84.0

In the case oxygen there is a $\gamma - \beta$ solid-solid transition in the bulk at 43.8 K, and a corresponding transition at a lower temperature in the porous glass. These experimental studies are for pores filled with adsorbate.

There has been little in the way of systematic simulation studies of melting and freezing in pores so far, although studies are in progress [47, 48]. An example of a GCMC study for slit pores with structureless walls is shown in

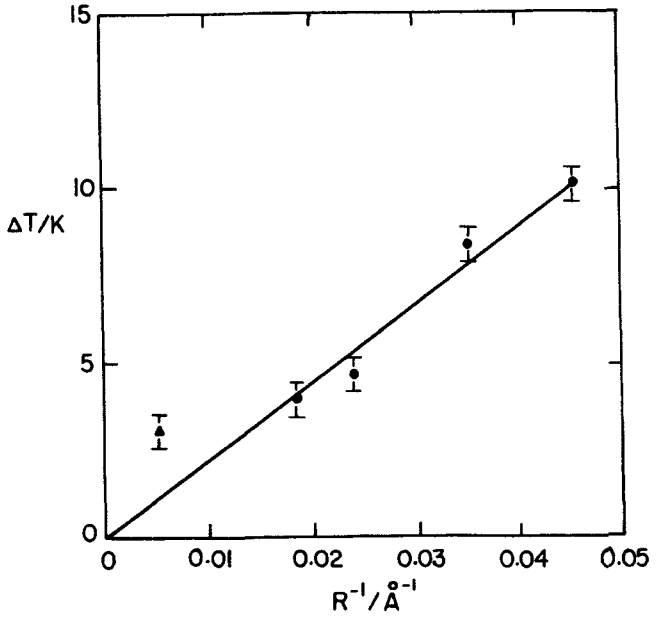

a

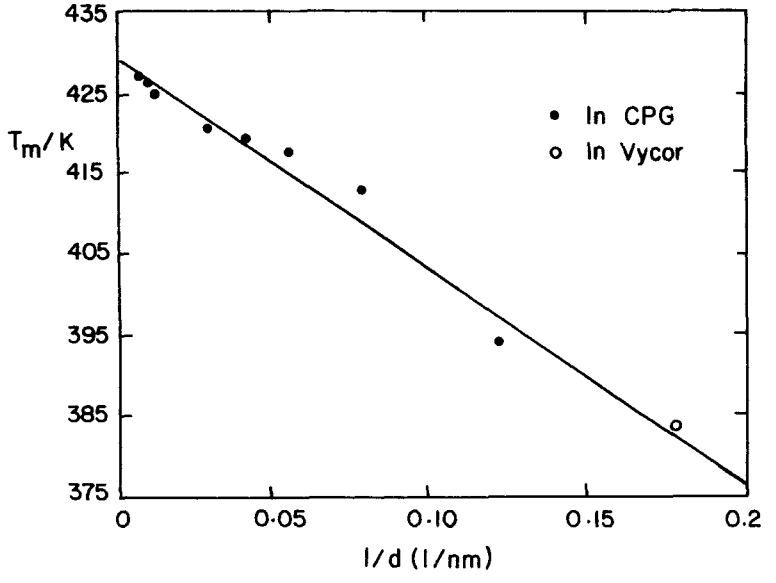

b

FIGURE 15 (a) Experimentally determined freezing point lowering, $\Delta T = T_f^{bulk} - T_f^{pore}$, for oxygen in sol-gel glasses with near monodisperse pore size distribution; R is the average pore radius. From Warnock *et al.* [39]; (b) melting temperatures for indium in porous silica glasses, with mean pore sizes from 6 to 141 nm, from differential scanning calorimetry [43].

Figure 3 [10], where FT means freezing transition. At the lower temperatures ($T^* = 0.4, 0.5, 0.6$), the monolayer formed at $\mu^*_{con} = -10.0$ is at first a fluid monolayer, but at somewhat higher pressures (chemical potentials) a freezing transition occurs. The freezing transition occurs at higher pressures as the temperature is increased, and is not observed for the temperatures studied above $T^* = 0.7$. The second layer shown in the adsorption isotherms of Figure 3 is solid-like at the lower temperatures, but at $T^* = 0.7$ it is fluid-like at the lower pressures, and a freezing transition is observed at somewhat higher pressures. For temperatures higher than 0.7 the second layer is fluid-like.

Some care is needed to locate freezing and melting transitions in the simulations, since the change in density observed in the adsorption isotherm is small and not a reliable indicator. Other indicators that are helpful in locating the transition are (a) snapshots of molecular configurations in a given layer of adsorbed molecules, (b) in-plane pair correlation functions or static structure factors, and (c) diffusion coefficients. All three of these properties were examined in connection with the freezing transitions shown in Figure 3. Snapshots of in-layer molecular configurations and pair correlation functions are shown for two-dimensional monolayer liquid and solid states for $T^* = 0.5$ and $H^* = 5$ in Figures 16 and 17, respectively. The results shown correspond to points C (fluid, just before freezing) and D (just after freezing) in Figure 3 (b). The configurations shown in Figure 16 show a fluid-like structure for point C, but a regular crystal array with some defects for D. Similarly, the pair

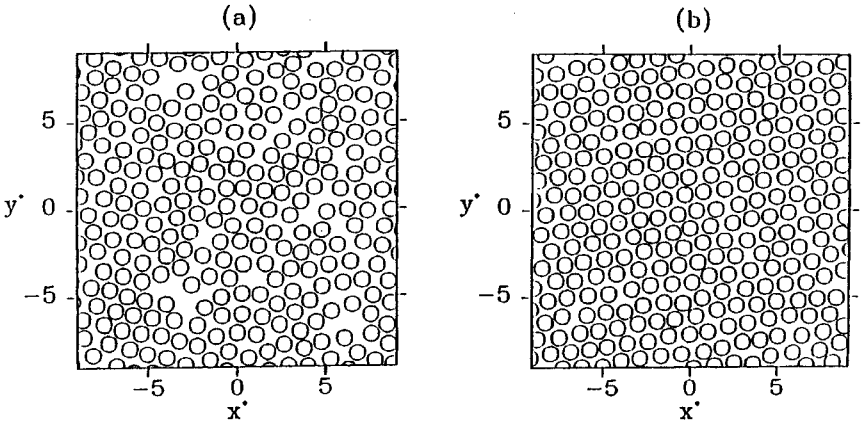

FIGURE 16 Snapshots of molecular positions from MD simulations of the contact layer for the system shown in Figure 3 (b), methane in a slit carbon pore of width $H^* = 5$ at $T^* = 0.5$, at (a) point C (fluid-like, $\rho_p^* = 0.313$), (b) point D (solid-like, $\rho_p{}^* = 0.348$). From Jiang *et al.* [10].

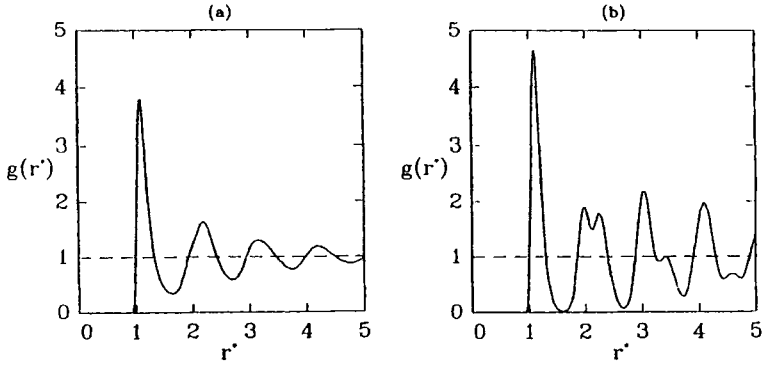

FIGURE 17 In-layer pair correlation functions, $g(r)$, for the same system as in Figure 16: (a) point C, (b) point D of Figure 3 (b). From Jiang *et al.* [10].

correlation functions shown in Figure 17 show a liquid-like structure for point C, but a solid-like one for point D. The self-diffusion coefficient at point D is about 300 times smaller than at point C, and gives a particularly clear picture of the freezing transition (Fig. 18).

A useful criterion for freezing is the Hansen-Verlet criterion [49], which predicts that freezing will occur when the ratio $S(k_0)/S(k=\infty) > \sim 2.7$, where $S(k)$ is the structure factor and k_0 is the k value at the first peak. Experimental data on freezing tend to confirm this criterion. For freezing in pores the criterion can be applied to individual molecular layers.

Both the simulation and experimental work indicates that the effect on the melting temperature is strongly dependent on the degree of pore filling. For submonolayer coverage, the melting point is usually lowered, whereas for a full monolayer the melting temperature apparently goes up [48]. For filled pores the melting temperature is usually lowered. This latter effect can be understood as follows. The molecules in the first adsorbed layer find it relatively easy to arrange themselves on the necessary crystal lattice, while fulfilling the constraint imposed by the walls. However, successive layers must conform to both the constraint of the walls and of the lattice of the underlying molecules; molecules in the center of the pore will find it difficult to meet both the lattice and wall constraints, leading to a lowering in the melting temperature. If this model is correct, one might expect that for carefully tailored pores the freezing might be enhanced, leading to a rise in the freezing temperature, although for slightly different pore sizes or geometries it is lowered.

The simulation studies reported so far have, for the most part, located the freezing and melting transitions through indicators such as the diffusion

coefficients and in-plane correlation functions. It would be desirable to calculate the free energies of each phase and so locate the true thermodynamic transition point. Methods for doing this are available [*e.g.* 50], although it is generally necessary to know the equilibrium crystal structure in advance. The examples quoted in Figures 3 and 16–18 are for a structureless wall. However, wall structure is known to have a significant effect on the liquid-solid

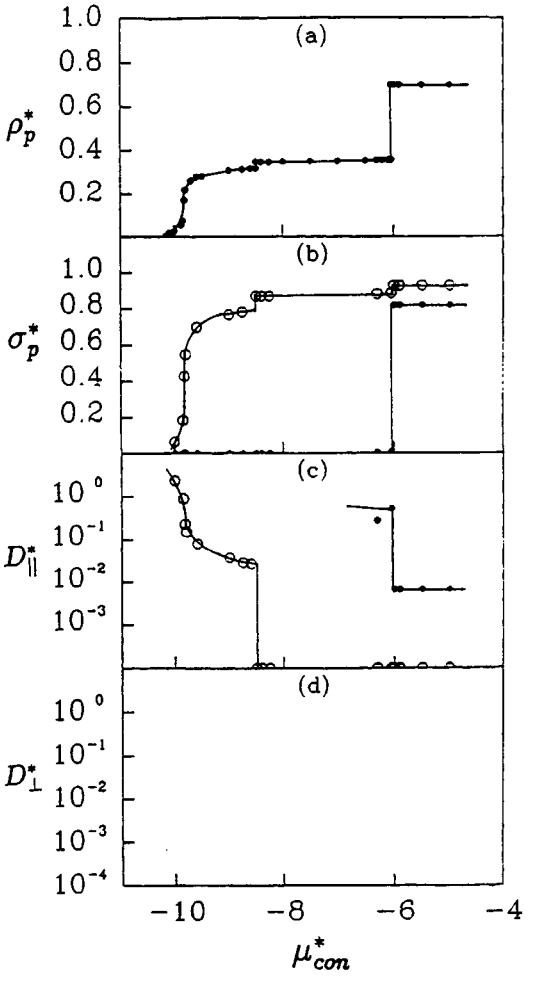

FIGURE 18 Adsorption and diffusion for the system shown in Figure 3 (b), methane in a slit carbon pore of width $H^* = 5$, $T^* = 0.5$: (a) volumetric adsorption isotherm; (b) adsorption per unit area; (c) diffusion coefficient parallel to the wall; (d) effective diffusion coefficeint perpendicular to the walls. Here $D^* = D/(\varepsilon_{ff}\sigma_{ff}^2/m)^{1/2}$. In figures (b) and (c) open circles represent the contact layer, while closed circles represent the inner layer. From Jiang *et al.* [10].

transition, even when the solid phase is not commensurate with the substrate. Some simulation studies have been reported for slit pores with structured walls [51, 52], and the solid-liquid transition has been shown to be sensitive to the registry of the two structured wall surfaces, and also to wall roughness. In simulations with structured walls care must be taken to choose the size of the surfaces so that the periodic boundary conditions match the symmetry of the external field. This point is further discussed in the next section.

6. SOLID-SOLID TRANSITIONS

Few experimental or simulation studies of solid-solid transitions in pores have been reported. However, there have been many studies of such transitions for monolayer or submonolayer coverages on single surfaces; a review of some of the simulation work for monolayers on basal plane graphite has been given by Steele [53]. An example of the results of such an experimental study of methane adsorption on a nonporous graphite surface [13] is shown in Figure 19. In addition to the two-dimensional gas-liquid and fluid-solid

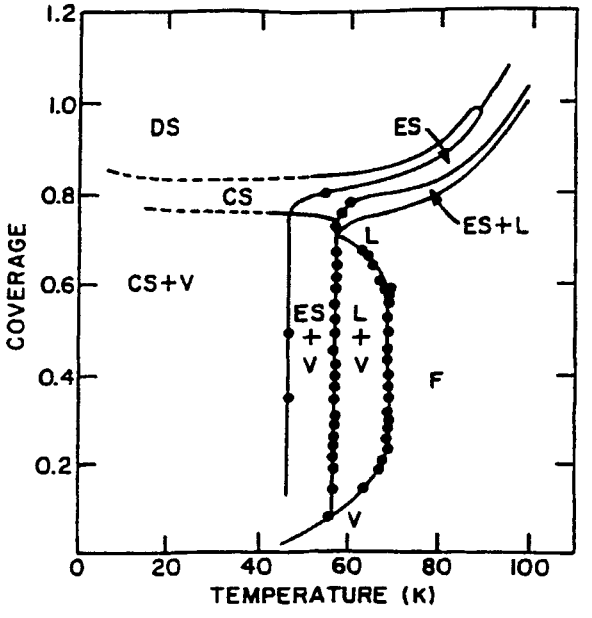

FIGURE 19 Phase diagram for methane on graphite from Kim *et al.* [13].

transitions, the system displays transitions between a commensurate solid (CS) and a dense incommensurate solid (DS) phase, as well as between the CS and an expanded solid (ES) phase. These transitions were found to be continuous in the pure solid phase near the complete monolayer. As seen in the phase diagram, there is a commensurate-incommensurate transtition (CIT) between CS and DS phases below 50 K, and the DS phase always locks into a commensurate region before changing into the ES phase between 50 and 88 K.

Jiang *et al.* [54] have reported a simulation study of the CIT for this system at conditions near the complete monolayer at 40.0 K. At these high surface densities it is difficult to carry out the successful molecule creation and destruction steps needed for GCMC simulations, and NVTMC simulations were therefore used. A structured wall was employed, and a solid-fluid potential with laterally varying periodicity based on the usual Fourier expansion truncated at first order [12] was used,

$$u_{sf}(x,y,z) = u_0(z) + u_1(z) f(x,y) \tag{7}$$

where $u_0(z)$ is the 10–4–3 potential,

$$u_0(z) = A\left[\frac{2}{5}\left(\frac{\sigma_{sf}}{z}\right)^{10} - \left(\frac{\sigma_{sf}}{z}\right)^{4} - \left(\frac{\sigma^4{}_{sf}}{3\Delta(0.61\Delta + z)^3}\right)\right] \tag{8}$$

where $A = 2\pi\rho_s\varepsilon_{sf}\sigma_{sf}^2\Delta$, z is the distance between a fluid molecule and the substrate surface, Δ is the separation between lattice planes, ρ_s is the number density of the solid, and σ_{sf} and ε_{sf} are the parameters for the solid-fluid interaction, calculated with the Lorentz-Berthelot combining rules. The graphite parameters are $\sigma_{ss} = 0.340$ nm, $\varepsilon_{ss}/k = 28.0$ K, $\Delta = 0.335$ nm. The functions $u_1(z)$ and $f(x,y)$ are given by

$$u_1(z) = B\left[C\left(\frac{a_1}{z}\right)^5 K_5\left(\frac{4\pi z}{\sqrt{3}a_1}\right) - D\left(\frac{a_1}{z}\right)^2 K_2\left(\frac{4\pi z}{\sqrt{3}a_1}\right)\right] \tag{9}$$

$$f(x,y) = -2\left[\cos 2\pi\left(\frac{x}{a_1} + \frac{y}{\sqrt{3}a_1}\right) + \cos 2\pi\left(\frac{x}{a_1} - \frac{y}{\sqrt{3}a_1}\right) + \cos\frac{4\pi y}{\sqrt{3}a_1}\right] \tag{10}$$

where $B = 4\pi\varepsilon_{sf}\sigma^6{}_{sf}/\sqrt{3}a_1^6$, $C = \sigma^6{}_{sf}/30a_1^6(2\pi/\sqrt{3})^5$, $D = 2(2\pi/\sqrt{3})^2$, and $a_1 = 0.246$ nm. K_1 and K_2 are modified Bessel functions of the second kind.

The above potential neglects several effects, including three-body terms, anisotropic polarizability of the surface atoms, etc. For this reason, Jiang *et al.*

also considered a modified form of the truncated Fourier expansion of eqn. (7),

$$u_{sf}(x, y, z) = u_0(z) + \lambda u_1(z) f(x,y) \tag{11}$$

where λ is a parameter that enables the corrugation of the wall potential to be varied.

The unit cell of the graphite lattice used by Jiang *et al.* [54] contains 6 hexagon sites, and is shown in Figure 20. It is chosen to meet the requirement that the periodic boundary conditions match the symmetry of the external field. This is straightforward when the adsorbed solid monolayer is commensurate with the underlying graphite lattice, but more care is needed with incommensurate adsorbed phases, since they have a different periodicity to that of the lattice [55–57]. In the study of Jiang et al. the estimate by Bruch [58] of the smallest lattice constant of a 2D solid for monolayer methane on graphite, 0.490 nm, was used, and the adsorbent surface was constructed from

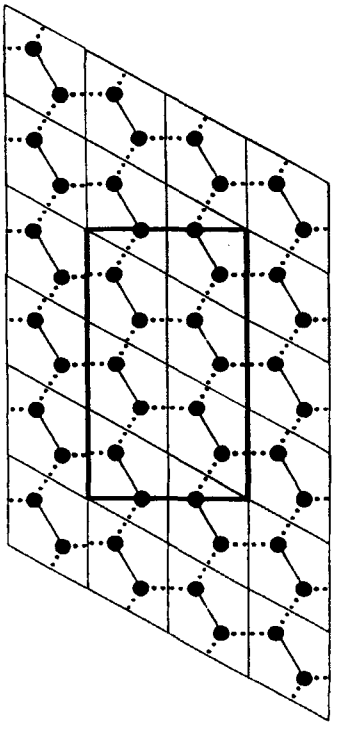

FIGURE 20 Unit cell of the graphite lattice, indicated by the bold line. Solid points denote carbon atoms. From Jiang *et al.* [54].

a 12 × 25 array of unit cells, giving the surface dimensions of 8.854 × 10.65 nm. On this surface a compressed monolayer (DS phase) contained 650 molecules, while a commensurate monolayer contained 600 molecules. The simulations were started with N molecules randomly distributed over the surface; typical runs were of about 100,000 steps per molecule, with runs that were several times longer for points near phase transitions.

Results from these simulations in the region near the commensurate-incommensurate transition are shown in Figures 21–24. In Figure 21 is shown the average of the quantity $f = -f(x,y)/2$ where $f(x,y)$ is given by Eqn. (10). The quantity $\langle f \rangle$ is a useful indicator of the strength of epitaxy [57]. It takes the value 3 for a perfect epitaxial phase, and 0 for a random incommensurate phase, and is plotted against the coverage θ, defined such that a perfect commensurate monolayer corresponds to $\theta = 1$. The CIT is indicated by the sharp decrease in $\langle f \rangle$ at $\theta = 1$. The value of $\langle f \rangle$ is seen to be about 2.5 for coverages below $\theta = 1$, to drop sharply at $\theta = 1$ to a value of about 1.5, and to decrease further after that. GCMC simulations were used to determine the lower coverage limit of the commensurate phase. This limit was found to be at

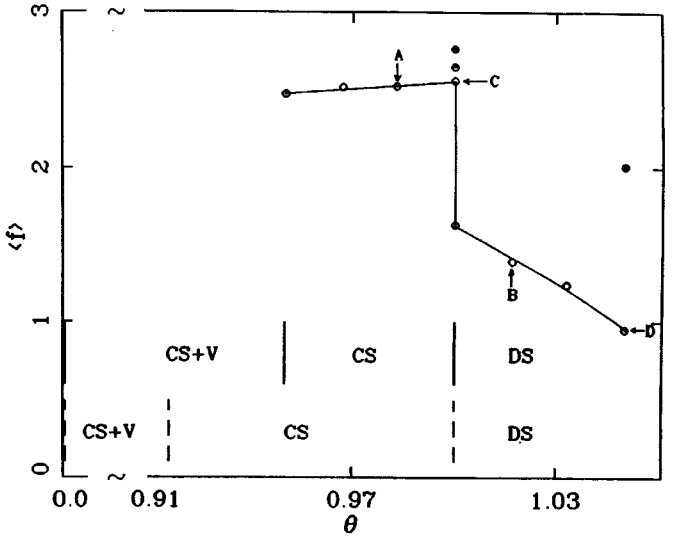

FIGURE 21 The function $\langle f \rangle$ versus coverage θ for methane on graphite at 40.0 K from NVTMC simulations; $\theta = 1$ corresponds to a full commensurate monolayer coverage. Simulations with $\lambda = 1$, 2 and 4 are denoted by empty, half-filled and solid circles, respectively; lines are drawn as a guide to the eye. Solid and dashed vertical lines show phase boundaries from simulation and experiment, respectively: CS = commensurate solid, V = vapor, DS = dense incommensurate solid phase. Experimental results are from Kim *et al.* [13]. Taken from Jiang *et al.* [54].

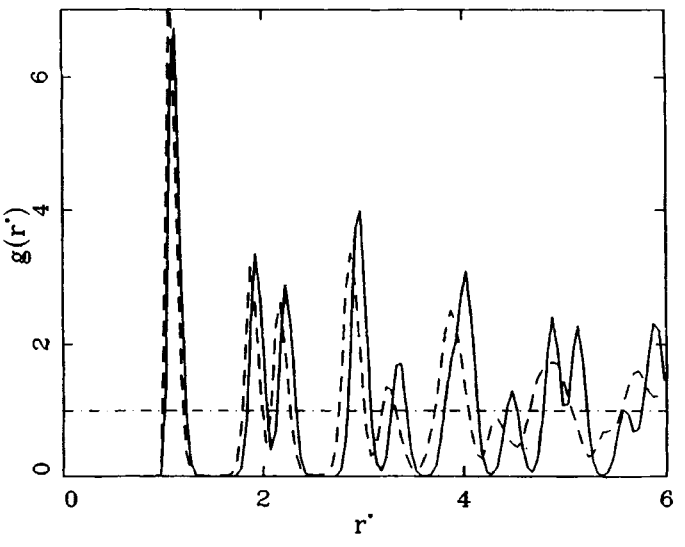

FIGURE 22 In-layer pair correlation functions for monolayer methane adsorbed on graphite at 40.0 K, from NVTMC simulations, for the points C (solid line, CS) and D (dashed line, DS) of Figure 21. From Jiang *et al.* [54].

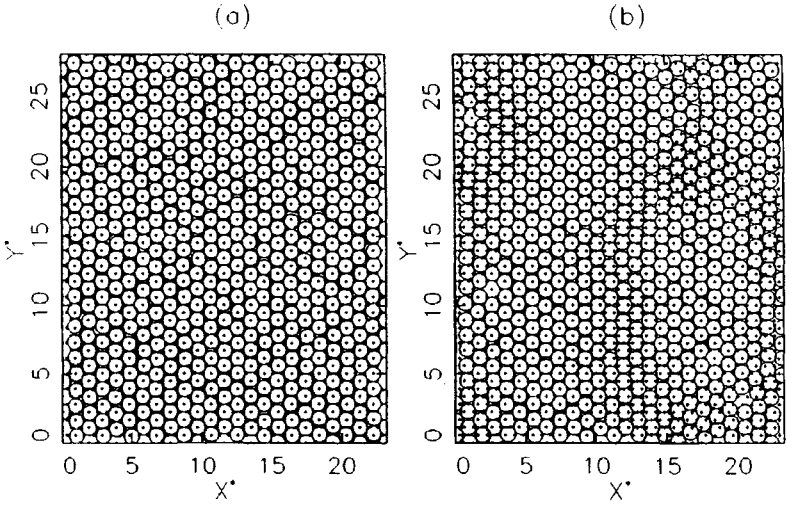

FIGURE 23 Snapshots of molecular positions for monolayer methane on graphite at 40.0 K at points (a) C (CS), and (b) D (DS) of Figure 21. Adsorption sites are shown by crosses. From Jiang *et al.* [54].

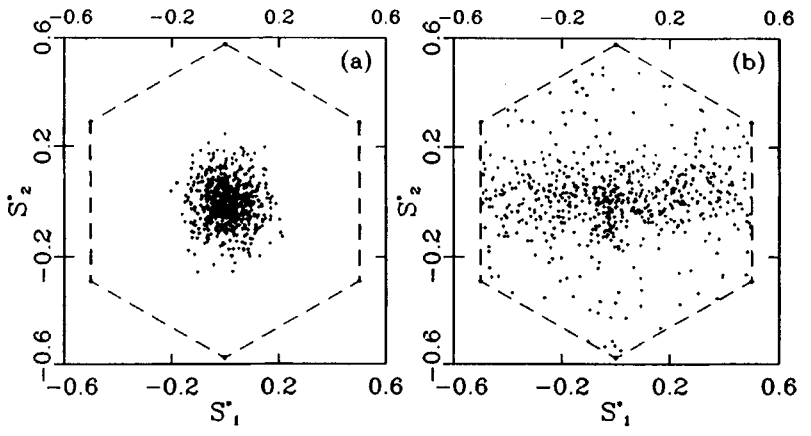

FIGURE 24 The density of dots over a graphite hexagon shown in the figure is proportional to the density of methane molecules above the equivalent positions on the graphite surface ($T = 40.0$ K) for points (a) C (CS) (b) D (DS) of Figure 21. S_1 and S_2 are in the lattice symmetry coordinates. From Jiang *et al.* [54].

$\theta = 0.95$ in the simulations (at 40 K), as compared to an experimental finding [13] of $\theta = 0.91$ at 45 K. Thus, below $\theta = 0.95$ the simulations show vapor coexisting with a commensurate solid phase, between $\theta = 0.95$ and $\theta = 1.00$ a single commensurate phase, and above $\theta = 1.00$ a dense solid phase. This is in qualitative agreement with the experimental data [13]. Increasing λ from 1 to 2 or 4 made the commensurate phase more stable at $\theta = 1.00$, as expected, but for larger θ values it was found that it could change the dense incommensurate monolayer to a more commensurate one by pushing some molecules out of the first layer and into a second one. Thus for $\theta = 1.05$ there were 627 molecules in the first, and 3 in the second layer for $\lambda = 1$, while there were 612 and 18 molecules in these layers for $\lambda = 4$. Thus increasing λ decreased the compression of the monolayer.

Other indicators of the CIT transition are shown in Figures 22–24, where properties are compared for the points C (commensurate phase, just before the transition) and D (dense incommensurate phase, after transition) of Figure 21. The in-layer pair correlation functions given in Figure 22 show the compression of the structure of the monolayer on going from the CS to DS phase. In Figure 24 the density of the dots over the graphite hexagon is proportional to the density of methane molecules above the equivalent positions on the graphite surface, and shows vividly the different character of the CS and DS phases.

7. CONCLUSIONS

There have been numerous simulation studies of capillary condensation and wetting in pores of simple geometry (slits, cylinders, etc.) with homogeneous surfaces over the last decade, and the effect of confinement on these transitions is now rather well understood. The GCMC and GEMC methods are the most commonly used for equilibrium properties, although MD remains useful, especially when the dynamical behavior or the interface between the two equilibrium phases is of interest. Even for these transitions there is a need for more work in several areas, including finite size effects near the critical region, and the dynamics of phase separation in pores. Much remains to be understood about the influence of surface heterogeneity and pore networking on phase transitions. As yet there seem to be no very systematic studies of the influence of these factors, although they are likely to play a major role in most real materials. There is also a need for work on the effects of confinement on other phase transitions, including liquid-liquid, solute solubilities, melting and freezing, and solid-solid transitions. These transitions are of considerable scientific and practical improtance, but very little is yet known about their nature in porous media.

The great majority of the simulation work so far has inferred phase transitions through observation of order parameters (*e.g.* discontinuities in adsorption, diffusion rates, etc.). Only in a few cases have the free energies, and hence the true thermodynamic phase transition, been calculated. Since large hysteresis effects and metastable states are a common feature of confined fluids, future studies should include calculations of the thermodynamic phase transition.

The experimental situation in this field remains unsatisfactory, since most studies have been for poorly characterized porous materials. Although there have been some exceptions [*e.g.* 2, 13, 24, 25], there is a strong need for more careful experimental work on well understood materials in which the pore sizes and dimensions are known, so that direct comparisons with the simulations can be used to validate and refine the models.

Acknowledgements

We are grateful to the National Science Foundation for support of this research (grant no. CTS-9508680), and also for support of our international cooperation through grants from the NSF U.S./Poland (INT-9511946) and U.S./Korea (grant no. INT-9302837) cooperative research programs. Super-

computer time was provided under an NSF Metacenter grant (No. MCA93S011P).

References

[1] The literature on DFT and simulation studies of phase transitions in pores is too extensive to review here. An overview of some typical recent work can be found in the proceedings of the Fundamentals of Adsorption Conferences, held every three years. *See Proceedings of the Fourth International Conference on Fundamentals of Adsorption*, ed. Suzuki, M., Engineeing Foundation, New York (1993). *Proceedings of the Fifth International Conference on Fundamentals of Adsorption*, ed. LeVan, M. D. in press (1996).

[2] Findenegg, G. H., Gross S. and Michalski, T. (1994). *Characterization of Porous Solids* III, Elsevier, Amsterdam, ed. J. Rouquerol, 71, M. Thommes and G. H. Findenegg, (1994); "Pore Condensation and Critical-Point Shift of a fluid in Controlled-Pore Glass," *Langmuir*, **10**, 4270.

[3] Allen, M. P. and Tildesley, D. J. (1987). *Computer Simulation of Liquids*, Clarendon Press, Oxford, 49.

[4] Mezei, M. and Beveridge, D. L. (1987). *Ann. New York Acad. Sciences*, **482**, 1.

[5] Gubbins, K. E. (1989) "The role of computer simulation in studying fluid phase equilibria", *Mol. Simulation*, **2**, 223.

[6] Frenkel, D. (1991). in *Computer Simulation in Materials Science*, Kluwer Academic, Dordrecht, eds. Meyer, M. and Pontikis, V. 85.

[7] Panagiotopoulos, A. Z. (1995). in *Observation, Prediction and Simulation of Phase Transitions in Complex Fluids*, Kluwer Academic, ed. Baus, M. *et al.*, 463.

[8] Gubbins, K. E. (1994) in *Models for Thermodynamic and Phase Equilibrium Calculations*, Dekker, New York, ed., Sandler, S. I. 507.

[9] Peterson, B. K. and Gubbins, K. E. (1988). "Phase transitions in a cylindrical pore: Grand canonical Monte Carlo, mean field theory and the Kelvin equation", *Mol. Phys.*, **62**, 215 (1987). Peterson, B. K., Gubbins, K. E., Heffelfinger, G. S., Marini Bettolo Marconi, U. and Van Swol, F. "Lennard-Jones fluids in cylindrical pores: Non local theory and computer simulation", *J. Chem. Phys.*, **88**, 6487 (1988).

[10] Jiang, S., Rhykerd, C. L., Gubbins, K. E. (1993) "Layering, freezing transitions, capillary condensation and diffusion of methane in slit carbon pores", *Mol. Phys.*, **79**, 373.

[11] Heffelfinger, G. S., Van Swol, F. and Gubbins, K. E. (1987) "Liquid-vapour coexistence in a cylindrical pore", *Mol. Phys.*, **61**, 1381.

[12] Steele, W. A. (1974). *The Interaction of Gases with Solid Surfaces*, Pergamon, Oxford.

[13] Kim, H. K., Zhang, Q. M. and Chan, M. H. (1986). "Nonwetting growth and cluster formation of CF_4 on graphite", *Phys. Rev.* B, **34**, 4699.

[14] Abraham, F. F., Schreiber, D. E., Mruzik M. R. and Pound, G. M. (1976) "Phase separation in fluid systems by spinodal decomposition: a molecular-dynamics simulation", *Phys. Rev. Lett.*, **36**, 261.

[15] Maddox, M. W. and Gubbins, K. E. (1995) "Molecular simulation of fluid adsorption in Buckytubes", *Langmuir*, **11**, 3988.

[16] Müller, E. A., Rull, L. F., Vega, L. F. and Gubbins, K. E. (1996). "Adsorption or water on activated carbons: a molecular simulation study", *J. Phys. Chem.*, **100**, 1189.

[17] Johnson, J. K., Panagiotopoulos, A. Z. and Gubbins, K. E. (1994) "Reactive canonical Monte Carlo- A new simulation technique for reacting or associating fluids", *Mol. Phys.*, **81**, 717.

[18] Smith, W. R. and Triska, B. J. (1994) "The reaction ensemble method for the computer simulation of chemical and phase equilibria. 1. Theory and basic examples", *J. Chem. Phys.*, **100**, 3019.

[19] Tsangaris, D. M. and De Pablo, J. J. (1994) "Bond-bias simulation of phase equilibria for strongly associating fluids *J. Chem. Phys.*, **101**, 1477.

[20] Busch, N. A., Wertheim, M. S., Chiew, Y. C. and Yarmush, M. L. (1994) "A Monte Carlo method for simulating associating fluids", *J. Chem. Phys.*, **101**, 3147.

[21] Walker, P. L. and Janov, J. J. (1968) "Hydrophilic oxygen complexes on activated graphon", *J. Colloid Interface Sci.*, **28**, 449.
[22] Baudu, M., Le Cloirec, P. and Martin, G. (1993) "First approach of desorption energies of water and organic molecules onto activated carbon by differential scanning calorimetry studies", *Wat. Res.*, **27**, 69.
[23] Buczec, B., Swiatkowski, A. and Goworek, J. (1995) "Adsorption from binary liquid mixtures on commercial activated carbons", *Carbon*, **33**, 129.
[24] Sliwinska-Bartkowiak, M. paper presented at *Liblice 4 Conference on Statistical Mechanics of Liquids*, Milovoy, Czech Republic, June 1994.
[25] Sliwinska-Bartkowiak, M., Sowers, S. L. and Gubbins, K. E. (1996) *Langmuir*, in press.
[26] Christenson, H. K. and Blom, C. E.(1987) "Calculation of radial distribution functions for molecules in excited vibrational states", *J. Chem. Phys.*, **71**, 192.
[27] Reich, S. and Cohen, Y. (1981) "Phase separation of polymer blends in thin films", *J. Polymer Sci. Polymer Physics Ed.*, **19**, 1255.
[28] Budkowski, A., Steiner, U. and Klein, J. (1992) "The effects of confinement and surface interactions on coexistence in a binary polymer mixture", *J. Chem. Phys.*, **97**, 5229.
[29] Bruder, F. and Brenn, R. (1992) "Spinodal decomposition in thin films of a polymer blend", *Phys. Rev. Lett.*, **69**, 624.
[30] Lin, M. Y., Sinha, S. K., Drake, J. M., and Wu, X-I Thiyagarajan, P. and Stanley, H. B. (1994) "Study of phase separation of a binary fluid mixture in confined geometry", *Phys. Rev. Lett.*, **72**, 2207.
[31] Góźdź, W. T., Gubbins, K. E. and Panagiotopoulos, A. Z. (1995) "Liquid-liquid phase transitions in pores", *Mol. Phys.*, **84**, 825.
[32] Kierlik, E., Fan, Y., Monson, P. A. and Rosinberg, M. L. (1995) "Liquid-liquid equilibrium in a slit pore; Monte Carlo simulation and mean field density functional theory", *J. Chem. Phys.*, **102**, 3712.
[33] Panagiotopoulos, A. Z. (1994) "Molecular simulation of phase coexistence: Finite-size effects and determination of critical parameters for two- and three-dimensional Lennard-Jones fluids", *Int. J. Thermophys*, **10**, 447 (1989); Georgoulaki, A. M. Ntouros, I. V. Tassios, D. P. and Panagiotopoulos, A. Z. (1994) " Mixtures: Simulation and van der Wals 1-fluid theory", *Fluid Phase Equil.*, **100**, 153.
[34] Stapleton, M. R. and Panagiotopoulos, A. Z. (1990) "Applications of excluded volume map sampling to phase equilibrium calculations in the Gibbs ensemble", *J. Chem. Phys.*, **92**, 1285.
[35] Kierlik, E., Fan, Y., Monson, P. A. and Rosinberg, M. L. (1995) "Liquid-liquid equilibrium in a slit pore; Monte Carlo simulation and mean field density functional theory", *J. Chem. Phys.*, **102**, 3712.
[36] Fan, Y., Finn, J. E. and Monson, P. A. (1993) "Monte Carlo simulation study of adsorption from a liquid mixture at states near liquid-liquid coexistence", *J. Chem. Phys.*, **99**, 8238.
[37] Kumar, S. K., Tang, H. and Szleifer, I. (1994) "Phase transitions in thin films of symmetric binary polymer mixtures", *Mol. Phys.*, **81**, 867.
[38] Tell, J. L. and Maris, H. J. (1983) "Specific heats of hydrogen, deuterium, and neon in porous Vycor glass", *Phys. Rev.*, B, **28**, 5122.
[39] Warnock, J., Awschalom, D. D. and Shafer, M. W. (1986) "Geometrical supercooling of liquid in porous glass", *Phys. Rev. Lett.*, **57**, 1753.
[40] Torii, R. H., Maris, H. J. and Seidel, G. M. (1990) "Heat capacity and torsional oscillator studies of molecular hydrogen in porous Vycor glass", *Phys. Rev. B*, **41**, 7167.
[41] Sokol, P. E., Ma, W. J., Herwig, K. W., Snow, W. M., Wang, Y., Koplik, J. and Banavar, J. R. (1992) "Freezing in confined geometries", *App. Phys. Iett.*, **61**, 777.
[42] Strange, J. H., Rahman, M. and Smith, E. G. (1993) "Characterization of porous solids by NMR', *Phys. Rev. Lett.*, **71**, 3589.
[43] Unruh, K. M., Huber, T. E. and Huber, C. A., (1993) "Melting and freezing behavior of indium metal in porous glasses", *Phys. Rev. B*, **48**, 9021.
[44] Molz, E., Wong, A. P. Y., Chan, M. H. W. and Beamish, J. R. (1995) "Freezing and melting of fluids in porous glasses", *Phys. Rev. B*, **48**, 5741 (1993).
[45] Klein, J. and Kumacheva, E., (1995) "Confinement-induced phase transitions in simple liquids", *Science*, **269**, 816.

[46] Duffy, J. A., Wilkinson, N. J., Fretwell, H. M., Alam, M. A. and Evans, R. (1995) *J. Phys. Cond. Matter*, **7**, L713.
[47] Dominguez, H. and Evans, R. private communication (1995).
[48] Maddox, M. and Gubbins, K. E. (1996) paper in preparation.
[49] Chaikin, P. M. and Lubensky, T. C. (1995) "Principles of Condensed Matter Physics", Cambridge Univ. Press, Cambridge, 192.
[50] Frenkel, D. and Ladd, A. J. C. (1984) "New Monte Carlo method to compute the free energy of arbitrary solids. Application to the fcc and hcp phases of hard spheres", *J. Chem. Phys.*, **81**, 3188.
[51] Schoen, M., Rhykerd, C. L., Diestler, D. J. and Cushman, J. H. (1989) "Shear forces in molecularly thin films", *Science*, **245**, 1223.
[52] Curry, J. E., Zhang, F., Cushman, J. H., Schoen, M. and Diestler, D. J., (1994) "Transient coexisting nanophases in ultrathin films confined between corrugated walls", *J. Chem. Phys.*, **101**, 10824.
[53] Steele, W. A. (1996) "Monolayers of Linear Molecules Adsorbed on the Graphite Basal Plane: Structures and Intermolecular Interactions", *Langmuir*, Jan. 15 issue (1996).
[54] Jiang, S., Gubbins, K. E. and Zollweg, J. A. (1993) "Adsorption, isosteric heat and commensurate-incommensurate transition of methane on graphite", *Mol. Phys.*, **80**, 103.
[55] Nicholson, D., Cracknell, R. F. and Parsonage, N. (1990) "Evaluation of a model potential function for Ar graphite interaction using computer simulation", *Molec. Simulation*, **5**, 307.
[56] Nicholson, D., Parsonage, N. and Rowley, L. A. (1981) "A grand ensemble Monte Carlo study of model epitaxial rare gas monolayers", *Mol. Phys.* **44**, 629.
[57] Whitehouse, J. S., Nicholson, D. and Parsonage, N. (1983) "A grand ensemble Monte Carlo study of krypton adsorbed on graphite", *Mol. Phys.*, **49**, 829.
[58] Bruch, L. W. (1987) "Monolayer solids of tetrahedral molecules" *J. Chem. Phys.*, **87**, 5518.